PROCEEDINGS A

royalsocietypublishing.org/journal/rspa

Research



Cite this article: Patnaik S, Semperlotti F. 2020 A generalized fractional-order elastodynamic theory for non-local attenuating media. *Proc. R. Soc. A* **476**: 20200200.

http://dx.doi.org/10.1098/rspa.2020.0200

Received: 23 March 2020 Accepted: 13 May 2020

Subject Areas:

applied mathematics, wave motion, mechanics

Keywords:

non-local media, elastic waves, Snell's Law, fractional calculus

Author for correspondence:

Fabio Semperlotti

e-mail: fsemperl@purdue.edu

Electronic supplementary material is available online at https://doi.org/10.6084/m9.figshare. c.5013521.

THE ROYAL SOCIETY

A generalized fractional-order elastodynamic theory for non-local attenuating media

Sansit Patnaik and Fabio Semperlotti

School of Mechanical Engineering, Ray W. Herrick Laboratories, Purdue University, West Lafayette, IN 47907, USA

SP, 0000-0001-8975-130X; FS, 0000-0002-8143-3902

This study presents a generalized elastodynamic theory, based on fractional-order operators, capable of modelling the propagation of elastic waves in nonlocal attenuating solids and across complex non-local interfaces. Classical elastodynamics cannot capture hybrid field transport processes that are characterized by simultaneous propagation and diffusion. The proposed continuum mechanics formulation, which combines fractional operators in both time and space, offers unparalleled capabilities to predict the most diverse combinations of multiscale, non-local, dissipative and attenuating elastic energy transport mechanisms. Despite the many features of this theory and the broad range of applications, this work focuses on the behaviour and modelling capabilities of the space-fractional term and on its effect on the elastodynamics of solids. We also derive a generalized fractional-order version of Snell's Law of refraction and of the corresponding Fresnel's coefficients. This formulation allows predicting the behaviour of fully coupled elastic waves interacting with non-local interfaces. The theoretical results are validated via direct numerical simulations.

1. Introduction

Recent theoretical and experimental studies have shown that transport processes in complex media are often characterized by either hybrid or anomalous mechanisms. As an example, wave propagation in highly scattering (either periodic [1] or random [2]) media is characterized by a diffused field that coexists with the propagating component. This dual mechanism is often referred to as hybrid transport [3–5]. Depending on the structure of the medium, the diffusive component can follow classical Fourier [6] or Fickian [7,8] Laws associated

with Gaussian distributions; but it can also diverge significantly from them giving rise to anomalously diffusive mechanisms associated with heavy-tailed distributions. The present study will be limited to the analysis of wave propagation in complex elastic solids. In such class of media, anomalous behaviour has been observed, to name a few, in layered or porous media [9–11], cracked or damaged materials [12,13], natural soil [14], and biomedical materials like bones and tissues [15]. Propagation of waves in real media is characterized by both dissipation (typical of lossy media) and attenuation (due to frequency dispersion) that vary according to the specific material and geometric configurations. Several studies have highlighted a power-law dependence of the attenuation in many types of lossy media, including fractal and porous materials [16,17], animal tissues [16] and even molten rocks [18]. Anomalous attenuation has been observed in several (non-lossy) scattering media, particularly those characterized by fractal or random structures [2,19]. The coexistence of different spatial scales results in a dependence of the constitutive relations on the wavenumber, which renders the elastodynamic response fully non-local [20].

Seminal works from Eringen [20,21] have explored the role of non-locality in elasticity and laid its theoretical foundation. Later, several theories were proposed including those based on gradient and integral methods. Gradient elasticity theories [22,23] account for non-local behaviour by introducing strain or stress gradient-dependent terms in the stress–strain constitutive law. Integral methods [24,25] model non-local effects by defining the constitutive law in the form of a convolution integral between the strain and spatially dependent elastic properties. Although some of the physical behaviours described above have been addressed by selected methods, a comprehensive elastodynamic theory capable of capturing and simulating the complex interplay between these transport mechanisms is not available. It follows that the modelling of multimodal wave transport in complex media is still a very challenging task.

In recent years, fractional calculus has emerged as a powerful mathematical tool to model a variety of non-local, multiscale and anomalous phenomena. Fractional derivatives, being a differintegral type of operator, are intrinsically multiscale and provide a natural way to account for both non-local and memory effects. In the context of elasticity, space-fractional derivatives have been used to formulate non-local constitutive laws [26–32] and to account for long-range cohesive forces [33,34]. In the context of wave propagation, fractional models have helped modelling dissipation in lossy media using time-fractional derivatives [16,35–37]. More recently, space-fractional derivatives have been employed to capture attenuation in media exhibiting long-range cohesive forces [29,34,38] and even bandgaps in periodic media [39].

In the present work, we obtain the wave equation for a non-local media by starting from a frame invariant and thermodynamically consistent fractional continuum formulation. We show that the fractional model establishes a clear dependence between the order of the fractional derivative and the length scale (horizon of non-locality) which ultimately depend on the attenuation characteristics of the medium. The overall goal of this study is three fold. First, we present a comprehensive fractional-order elastodynamic formulation capable of incorporating in a unified framework several complex transport mechanisms. We highlight here that, while the fractional continuum formulation developed in this study builds upon [27,28], in our study, we have generalized the formulation in order to account for asymmetric horizon conditions that typically occur near geometric/material boundaries or interfaces. This is particularly important in the context of the second goal of this study that is to formulate a non-local Snell's Law enabling the theoretical prediction of refraction of elastic waves at non-local interfaces. Finally, we validate the non-local Snell's Law by considering the example of a practical physical system that can be effectively described by the fractional-order elastodynamic model.

2. Non-local continuum formulation using fractional calculus

The fractional-order continuum formulation presented below expands and generalizes the concept of classical non-local elasticity to its fractional-order counterpart and addresses key limitations of gradient and integral formulations. Although gradient elasticity theories provide

a satisfactory description of non-local behaviour (including some constitutive parameters depending on the material micro structure), they introduce serious difficulties when enforcing the boundary conditions associated with the strain gradient-dependent terms [22,23]. This latter aspect is particularly challenging in media like porous, cracked and fractal materials. On the other side, the integral methods are better suited to deal with boundary conditions but impose restrictions on the kernel used in the stress–strain relation [24]. It is shown in [40] that instabilities in integral methods are avoided if the Fourier transform of the kernel is positive everywhere. Note that the kernel used in fractional derivatives is positive everywhere. Additionally, in the context of slender structures, the classical integral approaches lead to mathematically ill-posed governing equations which leads to erroneous predictions such as absence of non-local effects and hardening behaviour for certain combination of boundary conditions [41,42]. In this class of problems, the ill-posedness stems from the fact that the constitutive relation between the bending moment field and the curvature is a Fredholm integral of the first kind, whose solution does not generally exists and if it exists, is not necessarily unique [41,42].

Remarkably, by formulating the deformation gradient tensor in a space-fractional form, the resulting theory can effectively combine features characteristic of both gradient and integral-based methods. It was established in [43] that the fractional-order non-local model gives rise to a self-adjoint and positive-definite system accepting a unique solution. Consequently, the fractional-order approach to non-local elasticity does not encounter mathematical ill-posedness and predicts a consistent softening behaviour of non-local slender structures irrespective of the nature of the boundary conditions [30,43]. Note also that, unlike gradient-based methods, additional boundary conditions are not required when the fractional derivative is defined in Caputo form. Further, in contrast to classical non-local approaches, the fractional-order formulation allows for a strong localized application of all thermodynamic balance laws [44].

Further, the fractional-order model of non-local elasticity enables modelling of hybrid transport mechanisms as well as anomalous attenuation-dispersion behaviour often linked to the coexistence of different spatial and temporal scales. From a general perspective, the space-fractional deformation gradient tensor can be interpreted as a fractional homogenization approach that is capable of capturing the non-local behaviour of complex attenuating solids and interfaces while greatly simplifying the treatment of boundary conditions. Recently, the second-gradient [45] and the relaxed micromorphic approaches [46,47] have been explored to account for dispersion in micro-structured media. However, these approaches usually lead to nonlinear governing equations. This is unlike the fractional-order governing equations of the non-local continuum developed in this study, which remain linear in nature and thus provide unique opportunities to extend important tools from theory of linear differential equations (e.g. the principle of superposition). This characteristic has several ramifications, particularly in the perspective of obtaining closed form relations for selected properties. More specifically, for the problem treated in this study, the fractional framework allows obtaining the attenuationdispersion relations for complex materials exhibiting anomalous behaviour due to either geometrical or material inhomogeneities. The same approach also enabled the reformulation and validation of the analogue to the traditional Snell's Law of refraction for complex interfaces.

(a) Fractional deformation gradient

In analogy with the traditional continuum approach to mechanics, the deformation analysis of a non-local solid can be performed by introducing two stationary configurations, namely, the reference (undeformed) and the current (deformed) configurations. Coordinates in the reference configuration are denoted by X and in the current configuration by x. The motion of the body from the reference configuration to the current configuration at any instant of time t is given as:

$$x = \psi(X, t), \tag{2.1}$$

such that $\psi(X,t)$ is a continuous and invertible mapping operation. In the initial configuration, the relative position of two point particles located at P and Q in the non-local medium is denoted

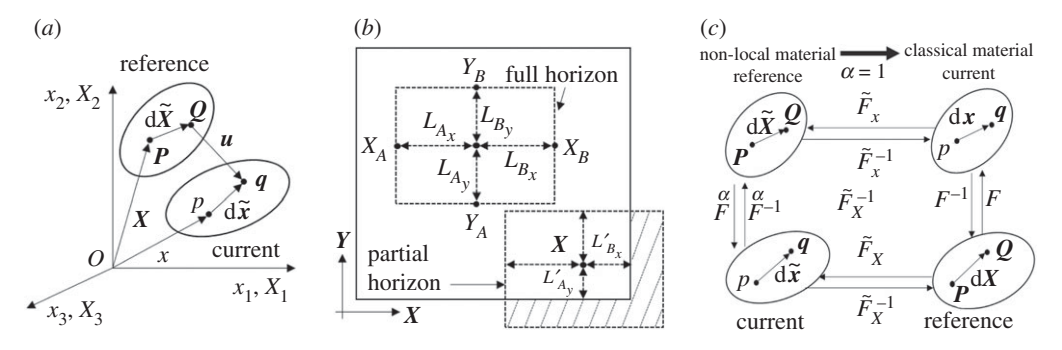


Figure 1. (a) Schematic of the infinitesimal material $(d\tilde{X})$ and spatial $(d\tilde{x})$ line elements in the non-local medium under the displacement field u. (b) Horizon of non-locality and length scales at different material points. The non-local model can account for a partial (i.e. asymmetric) horizon that occurs at a generic point X close to a boundary or a material interface. (c) Relations between the material and spatial line elements in the non-local medium $(d\tilde{X})$ and $d\tilde{X}$ and $d\tilde{X}$ and in the local medium $d\tilde{X}$. The schematic (c) is adapted from [27].

by $d\tilde{X}$ (figure 1). After deformation, the particles move to new positions p and q, such that the relative position vector is $d\tilde{x}$. $d\tilde{X}$ and $d\tilde{x}$ are the material and spatial differential line elements in the non-local medium, conceptually analogous to the classical line elements.

In the classical continuum description, the differential line elements in the reference and current configurations, dX and dx, are related using the deformation gradient tensor:

$$dx = \left[D_X^1 \psi(X, t) \right] dX = \left[F(X, t) \right] dX, \tag{2.2}$$

where $D_X^1(\cdot)$ denotes the first integer-order spatial derivative with respect to the reference coordinates. In order to describe the non-local continuum, we model non-locality in the differential line elements of the non-local medium by imposing a fractional-order transformation on the line elements of the local medium. More specifically, space-fractional gradients are used to map the differential line elements in the local medium to the non-local medium in the following manner:

$$d\tilde{x} = \left[D_X^{\alpha} \psi(X, t) \right] dX = \left[\tilde{F}_X(X, t) \right] dX \tag{2.3a}$$

and

$$d\tilde{X} = \left[D_x^{\alpha} \psi^{-1}(x,t)\right] dx = \left[\tilde{F}_x(x,t)\right] dx \tag{2.3b}$$

where $D_X^{\alpha}\psi$ is a space-fractional derivative whose details will be discussed below. Given the differ-integral nature of the space-fractional derivatives, the differential line elements $\mathrm{d}\tilde{X}$ and $\mathrm{d}\tilde{x}$ are non-local in nature. Using the definitions for $\mathrm{d}\tilde{X}$ and $\mathrm{d}\tilde{x}$, the fractional deformation gradient tensor F with respect to the non-local coordinates can be derived. Note from equation (2.3) that F_X and F_X transform as vectors and hence, are two-point tensors. Consequently, by using the classical chain rule and equations (2.2) and (2.3), F is found as:

$$\frac{\mathrm{d}\tilde{x}}{\mathrm{d}\tilde{X}} = \tilde{F} = \tilde{F}_X F^{-1} \tilde{F}_x^{-1}.$$
 (2.4)

A visual interpretation of the mapping operations between local and non-local configurations is given in figure 1*c*. Note that, although the deformation gradient tensor builds upon a previous theory proposed in [27,28], we start from a different definition of the fractional derivatives that has interesting implications for the resulting theory.

The fractional derivative $D_X^{\alpha}\psi(X,t)$ is a space-fractional Riesz–Caputo (RC) derivative of order $\alpha \in (0,1)$ defined on the interval $X \in (X_A, X_B) \subseteq \mathbb{R}^3$ in the following manner:

$$D_X^{\alpha} \psi(X,t) = \frac{1}{2} \Gamma(2-\alpha) \left[L_A^{\alpha-1} {}_{X_A}^C D_X^{\alpha} \psi(X,t) - L_B^{\alpha-1} {}_X^C D_{X_B}^{\alpha} \psi(X,t) \right]$$
(2.5a)

and

$$D_{X_{j}}^{\alpha}\psi_{i}(X,t) = \frac{1}{2}\Gamma(2-\alpha)\left[L_{A_{j}}^{\alpha-1}{}_{X_{A_{j}}}^{C}D_{X_{j}}^{\alpha}\psi_{i}(X,t) - L_{B_{j}}^{\alpha-1}{}_{X_{j}}^{C}D_{X_{B_{j}}}^{\alpha}\psi_{i}(X,t)\right],$$
 (2.5b)

where, ${}_{X_A}^C D_X^\alpha \psi$ and ${}_X^C D_{X_B}^\alpha \psi$ are the left- and right-handed Caputo derivatives, respectively. In equation (2.5), L_{A_j} and L_{B_j} are length scales in the jth direction in the reference configuration, and $\Gamma(\cdot)$ is the Gamma function. Note that the index j in equation (2.5b) is not a repeated index. In the current configuration, these length scales are denoted as l_{A_j} and l_{B_j} . The fractional deformation gradient defined in equation (2.4) is non-local due to the properties of the RC derivative. The interval of the derivative (X_A, X_B) defines the horizon of non-locality which is schematically shown in figure 1 for a generic point X in a two-dimensional (2D) domain.

Aside from providing an explicit parameter to define the range of non-locality, the length-scale parameters ensure the dimensional consistency of the deformation gradient tensor. Further, the factors $\frac{1}{2}\Gamma(2-\alpha)$, $L_{A_j}^{\alpha-1}$ and $L_{B_j}^{\alpha-1}$ allow ensuring the frame invariance of the formulation. We prove that the deformation gradient tensor is frame invariant for $L_{A_j} = X_j - X_{A_j}$ and $L_{B_j} = X_{B_j} - X_j$ in §2b. Thus, the horizon length $(X_{B_j} - X_{A_j})$ in the jth direction is $L_{A_j} + L_{B_j}$. We emphasize and prove in the following sections that the non-local formulation in equation (2.3) is more general than [27,28] because it enables an efficient and accurate treatment of frame invariance in the presence of asymmetric horizons, material boundaries and interfaces (figure 1b).

We make an important remark on the definition of the deformation gradient tensor for points lying on the boundaries of the solid. Consider, a material point X_0 lying on one of the boundaries identified by the normal in the jth direction such that $L_{A_i} = 0$. Under this limiting condition:

$$\tilde{F}_{X_{ij}} = \lim_{L_{A_j} \to 0} D_{X_j}^{\alpha} \psi_i = \frac{1}{2} \left[\left. \frac{\mathrm{d} \psi_i(\mathbf{X}, t)}{\mathrm{d} X_j} \right|_{X_0} + (1 - \alpha) L_{B_j}^{\alpha - 1} \int_{X_{0_j}}^{X_{B_j}} \frac{D_{S_j}^1 \psi_i(\mathbf{S}, t)}{(S_j - X_j)^{\alpha}} \mathrm{d} S_j \right]. \tag{2.6}$$

The detailed derivation of the above expression is provided in the electronic supplementary material. From equation (2.6), it is immediate to observe that while the right-handed Caputo derivative captures non-locality ahead of the point X_0 (in the jth direction), the left-handed derivative is reduced to the classical first-order derivative. This suggests that the truncation of the non-local horizon (and the corresponding convolution) at the boundary has been accounted for in a consistent manner. We emphasize that similar expressions hold when $L_{B_j} = 0$. Further, while the above is valid for \tilde{F}_X , similar expressions can be derived for \tilde{F}_X and \tilde{F} .

(b) Frame invariance of the fractional deformation gradient tensor

In the following, we establish the frame invariance of the fractional-order continuum formulation. Recalling the definition of the deformation gradient tensor, we must show that the individual terms in equation (2.4) are frame invariant. We start by investigating the frame invariance of \tilde{F}_X . Consider a rigid-body motion superimposed on the reference configuration of the body X as:

$$\chi = c(t) + Q(t)X,\tag{2.7}$$

where Q(t) is a proper orthogonal tensor denoting a rotation and c(t) is a spatially constant term representing a translation. Under this rigid-body motion, the fractional deformation gradient \tilde{F}_X^X should be an orthogonal tensor such that $\tilde{F}_X^{XT}\tilde{F}_X^X = \mathbf{I}$. More specifically, the fractional deformation

gradient tensor should transform as $\tilde{F}_X^{\chi} = Q$, similar to the classical continuum case, such that the strain measures are null. From the definition of \tilde{F}_X in equation (2.3), it follows that:

$$\tilde{F}_{X_{ij}}^{\chi} = \frac{1}{2} \Gamma(2 - \alpha) \left[\frac{L_{A_j}^{\alpha - 1}}{\Gamma(1 - \alpha)} \int_{X_{A_j}}^{X_j} \frac{D_{S_j}^1 \chi_i(S, t)}{(X_j - S_j)^{\alpha}} dS_j + \frac{L_{B_j}^{\alpha - 1}}{\Gamma(1 - \alpha)} \int_{X_j}^{X_{B_j}} \frac{D_{S_j}^1 \chi_i(S, t)}{(S_j - X_j)^{\alpha}} dS_j \right], \quad (2.8)$$

where *S* is a dummy vector variable in space. For the rigid-body motion χ , $D_{S_j}^1 \chi_i = Q_{ij}$. Using this result along with the relation $\Gamma(2-\alpha) = (1-\alpha)\Gamma(1-\alpha)$ in equation (2.8), we obtain:

$$\tilde{F}_{X_{ij}}^{\chi} = \frac{1}{2} \left[L_{A_j}^{\alpha - 1} (X_j - X_{A_j})^{1 - \alpha} + L_{B_j}^{\alpha - 1} (X_{B_j} - X_j)^{1 - \alpha} \right] Q_{ij}. \tag{2.9}$$

For $\tilde{F}_X^{\chi} = Q$ to hold for all time, $L_{A_j} = X_j - X_{A_j}$ and $L_{B_j} = X_{B_j} - X_j$. By repeating this procedure, it is immediate to show that the same arguments hold for the frame invariance of \tilde{F}_X^{χ} and subsequently of \tilde{F} . It is emphasized that the non-local formulation introduced through equations (2.3)–(2.5) allows for an exact treatment of frame invariance in the presence of asymmetric horizons which occurs at points close to material boundaries and interfaces. The different horizon lengths L_{A_j} and L_{B_j} enables the truncation of the horizon at points close to or on the boundary. These characteristics generalize the formulation previously presented in [27,28].

(c) Fractional strain

Analogous to classical strain measures, the fractional strain is defined using the difference in the scalar product of the differential line elements: $d\tilde{x}d\tilde{x} - d\tilde{X}d\tilde{X}$. Using equation (2.5), we obtain:

$$\overset{\alpha}{E} = \frac{1}{2} \left[\overset{\alpha}{F} \overset{\alpha}{F} \overset{\alpha}{F} - \mathbf{I} \right] \tag{2.10a}$$

and

$$\stackrel{\alpha}{e} = \frac{1}{2} \left[\mathbf{i} - \stackrel{\alpha}{F}^{-T} \stackrel{\alpha}{F}^{-1} \right], \tag{2.10b}$$

where $\overset{\alpha}{E}$ and $\overset{\alpha}{e}$ are the Lagrangian and Eulerian strain tensors in the non-local medium, and I and I are identity matrices. Now we obtain the expressions for the strain tensors in terms of the displacement gradients by using the kinematic position–displacement relations. The fractional-order gradient of the displacement field U(X) = x(X) - X is obtained using equation (2.3) as:

$$\nabla^{\alpha} \mathbf{U}_{X} = \tilde{\mathbf{F}}_{X} - \mathbf{I}. \tag{2.11}$$

The fractional gradient denoted by $\nabla^{\alpha} U_X$ is given as $\nabla^{\alpha} U_{X_{ij}} = D_{X_j}^{\alpha} U_i$. Similarly, the fractional displacement gradient in the Eulerian coordinates is given by:

$$\nabla^{\alpha} u_{\chi} = \mathbf{i} - \tilde{F}_{\chi}. \tag{2.12}$$

Using the non-local strain defined in equation (2.10) together with the equations (2.5), (2.11) and (2.12), the relationship between the strain tensors and displacement gradient tensors are obtained as:

$$\overset{\alpha}{E} = \frac{1}{2} \left[\nabla^{\alpha} \mathbf{U}_{X} + \nabla^{\alpha} \mathbf{U}_{X}^{T} + \nabla^{\alpha} \mathbf{u}_{x} + \nabla^{\alpha} \mathbf{u}_{x}^{T} - \nabla \mathbf{u} - \nabla \mathbf{u}^{T} + h.o.t \right]$$
(2.13a)

and

$$\stackrel{\alpha}{e} = \frac{1}{2} \left[\nabla^{\alpha} \boldsymbol{u}_{x} + \nabla^{\alpha} \boldsymbol{u}_{x}^{T} + \nabla^{\alpha} \boldsymbol{U}_{X} + \nabla^{\alpha} \boldsymbol{U}_{X}^{T} - \nabla \boldsymbol{U} - \nabla \boldsymbol{U}^{T} + h.o.t \right], \tag{2.13b}$$

where ∇U and ∇u are the classical displacement gradient tensors. For small deformations, the higher-order terms can be ignored and the infinitesimal fractional strain tensor is given by:

$$\tilde{\boldsymbol{\varepsilon}} = \frac{1}{2} (\nabla^{\alpha} \boldsymbol{U}_{X} + \nabla^{\alpha} \boldsymbol{U}_{X}^{T}) = \frac{1}{2} (\nabla^{\alpha} \boldsymbol{u}_{x} + \nabla^{\alpha} \boldsymbol{u}_{x}^{T}). \tag{2.14}$$

The relations in equations (2.13) and (2.14) are derived in the electronic supplementary material.

The compatibility condition for the strain-displacement fields in the fractional-order model for the non-local medium extends analogously from the classical compatibility relations as:

$$\nabla^{\alpha} \times \nabla^{\alpha} \times \tilde{\boldsymbol{\epsilon}} = 0, \tag{2.15}$$

where, $\nabla^{\alpha}(\cdot)$ denotes the fractional curl operator which is analogous to the classical curl operator but contains the RC derivatives. The fractional-order compatibility condition can be derived by considering the following fractional-order differentiation of the fractional-order strain tensor:

$$\tilde{\varepsilon}_{ij,\vec{k}\vec{l}} = \frac{1}{2} (u_{i,\vec{j}\vec{k}\vec{l}} + u_{j,\vec{i}\vec{k}\vec{l}}), \tag{2.16}$$

where $\tilde{\Box}$ indicates fractional-order differentiation. Through simple interchange of subscripts, we can generate the following additional relations:

$$\tilde{\varepsilon}_{kl,\overline{ij}} = \frac{1}{2} (u_{k,\overline{lij}} + u_{l,\overline{k}\overline{ij}}); \quad \tilde{\varepsilon}_{jl,\overline{ik}} = \frac{1}{2} (u_{j,\overline{lik}} + u_{l,\overline{jik}}); \quad \tilde{\varepsilon}_{ik,\overline{jl}} = \frac{1}{2} (u_{i,\overline{k}\overline{ij}} + u_{k,\overline{ij}\overline{l}}). \quad (2.17)$$

Working under the assumption of continuous displacements, we can interchange the sequence of the fractional-order differentiation in equations (2.16) and (2.17) and the displacement field can be eliminated to obtain: $\tilde{\epsilon}_{ij,\vec{k}l} + \tilde{\epsilon}_{kl,\vec{ij}} - \tilde{\epsilon}_{jl,\vec{ik}} - \tilde{\epsilon}_{ik,\vec{jl}} = 0$, which is equivalent to equation (2.15). Note that this is the necessary condition for compatibility. The sufficient nature of this condition follows from the application of the fractional Stokes theorem [48], analogous to the classical case.

(d) Fractional stress

Stress in a non-local isotropic medium is defined analogously to the local isotropic case as:

$$\tilde{\sigma}_{ij} = 2\mu \tilde{\varepsilon}_{ij} + \lambda \tilde{\varepsilon}_{kk} \delta_{ij}, \tag{2.18}$$

where λ and μ are Lamé constants of the solid. Traction \tilde{t} on a surface in the non-local solid with normal \hat{n} is defined analogous to the classical continuum formulation as:

$$\tilde{t}_i = \tilde{\sigma}_{ji} n_j. \tag{2.19}$$

The fractional-order continuum model presented above requires a few important remarks. First, it is evident that the fractional-order model presented above is based on a continuum mechanics approach. While this is a fundamental approach to mechanics and, in many aspects, analogous to classical and well-established continuum formulations, we introduce an important hypothesis by assuming a fractional-order formulation for the kinematics. More specifically, we define differential line elements using fractional-order deformation gradients similar to [27,28]. This hypothesis results in assuming that the response of a selected point within the solid is affected directly by the response of a collection of points within a characteristic volume, the so-called horizon of non-locality. Given that the fractional operator is applied directly to the displacement field via the deformation gradient, from a physical standpoint, the formulation accounts for long-range interactions that are proportional to the relative displacement of distant points within the horizon. This is indeed a possible formulation of the concept of actionat-a-distance that is often implemented in terms of long-range cohesive forces. Additional considerations on the physical meaning of fractional-order models can be found in [29,33,43].

Second, the fractional-order continuum formulation is thermodynamically consistent and it allows for a rigorous application of all thermodynamic principles. As shown in [44], the use of non-local fractional-order kinematic relations prevents the requirement of additional integral (non-local) constitutive stress–strain relations as seen in classical non-local approaches (e.g. [25]). As a result, the thermodynamic laws in the fractional-order theory are free from non-local residual terms. This greatly simplifies the constitutive modelling of the non-local solid while enabling a rigorous implementation of the thermodynamic laws at each point in the solid. The latter observation highlights an important benefit and a key motivation to pursue the fractional-order model of non-local elasticity. Recall that, classical non-local approaches allow

only a weak application (in a domain integral sense) and prevent the localized (point-wise) application of the thermodynamic balance laws. As discussed in [25], the weak application of thermodynamic balance laws, particularly the second law, leads to inconsistencies in the non-local continuum framework. As a result, the fractional-order continuum formulation is free from such thermodynamic inconsistencies.

Finally, we emphasize that all classical continuum relations are recovered from the fractional-order model when the order of the fractional derivative is set as $\alpha = 1$.

3. Elastodynamics of the non-local medium

The linear momentum balance equation in the non-local solid is derived by conservation principles analogous to the case of a local solid, and it is obtained as [27]:

$$\rho \frac{\mathrm{d}^2 u}{\mathrm{d}t^2} = \lambda \nabla (\nabla^\alpha \cdot u) + \mu \nabla \cdot \nabla^\alpha u + \mu \nabla \cdot \nabla^\alpha u^T + \tilde{f}, \tag{3.1}$$

where \tilde{f} is the external force vector, and $\nabla^{\alpha} \cdot \boldsymbol{u} = D_{X_k}^{\alpha} u_k$ is the fractional divergence. The space-fractional wave equation (3.1) can be further extended to include time-fractional derivatives as:

$$\rho \tau_0^{\beta - 2} \frac{\mathrm{d}^{\beta} \mathbf{u}}{\mathrm{d}t^{\beta}} = \lambda \nabla (\nabla^{\alpha} \cdot \mathbf{u}) + \mu \nabla \cdot \nabla^{\alpha} \mathbf{u} + \mu \nabla \cdot \nabla^{\alpha} \mathbf{u}^{T} + \tilde{\mathbf{f}}. \tag{3.2}$$

The time-fractional derivative in equation (3.2) is a left-handed Caputo derivative with order $\beta \in (1,2)$ which allows accounting for non-conservative dissipative effects such as those typical of frequency-dependent viscoelastic media. τ_0 is a time constant that maintains dimensional consistency of the wave equation. Lossy materials and time-fractional wave equations have been thoroughly studied in the literature. Hence we concentrate only on the space-fractional component and its effect on non-local elastodynamics.

An important remark should be made concerning the nature of the space- and time-fractional derivatives. Note that the double-sided RC derivative can only be used for fractional-order spatial differentiation and not for fractional-order temporal differentiation. In fact, the left-handed derivative is an operation performed on the past states (in time) or on points preceding a target point (in space), while the right-handed derivative is an operation performed on future states (in time) or on points following a target point (in space). Consequently, the use of a right-handed time-fractional derivative would render the formulation non-causal. Further, from a mathematical perspective, note that the right-handed fractional derivatives are conjugate to the left-handed derivatives. Consequently, a complete theory for fractional-order boundary value problems can only be developed when using both left- and right-handed space-fractional derivatives [49]. For the specific problem of non-local elasticity, both the left- and right-handed space-fractional derivatives are essential to capture a complete horizon of non-locality (figure 1b).

4. Dispersion relations and causality

To obtain the dispersion relation, we substituted in the space-fractional wave equation given in equation (3.1) the following ansatz:

$$u(x,t) = A_x e^{i(k_1 \cdot x - \omega t)} \hat{x} + A_y e^{i(k_2 \cdot x - \omega t)} \hat{y}, \tag{4.1}$$

where A_j is the wave amplitude in the jth direction (with j = x, y), ω is the angular frequency, and $k_1 = k_{1x}\hat{x} + k_{1y}\hat{y}$ and $k_2 = k_{2x}\hat{x} + k_{2y}\hat{y}$. The components of the wavevectors k_1 and k_2 are complex and they combine both compressional (P) and shear (S) wave components. Derivation of the dispersion relations requires the operation of the RC derivative that defines operators in equation (3.1) on the exponential functions in the assumed solution in equation (4.1). The RC

derivatives in equation (3.1) have lower and upper bounds at the respective terminals of the horizon of non-locality. When the fractional derivative has a lower bound of $-\infty$,

$${}_{-\infty}^{C}D_x^{\alpha}[e^{bx}] = b^{\alpha}e^{bx}, \tag{4.2}$$

the solution kernel of the fractional wave equation can be chosen in the form of exponential functions [39] corresponding to propagating plane waves. When lower bounds other than $-\infty$ are chosen, then solution kernels based on Mittag–Leffler functions are appropriate. However, under proper assumptions for the interval of the fractional derivative [39] both kernels satisfy the same dispersion relations. Similar comment holds for the upper bound. In the following, we choose exponential kernels given their simplicity and computational efficiency.

Using the RC derivative of the exponential given in equation (4.2), we obtain the complete form of the dispersion relations for compressional and shear waves in the non-local medium as:

$$-\rho\omega^{2}A_{x}e_{1} = i^{\alpha+1}\Gamma(2-\alpha)\left[(\lambda+2\mu)A_{x}\bar{l}_{x}^{\alpha-1}k_{1x}^{\alpha+1}e_{1} + \mu A_{x}\bar{l}_{y}^{\alpha-1}k_{1y}^{\alpha+1}e_{1} + \lambda A_{y}\bar{l}_{y}^{\alpha-1}k_{2y}^{\alpha-1}k_{2y}^{\alpha-1}k_{2x}e_{2} + \mu A_{y}\bar{l}_{x}^{\alpha-1}k_{2y}e_{2}\right]$$

$$(4.3a)$$

and

$$-\rho\omega^{2}A_{y}e_{2} = i^{\alpha+1}\Gamma(2-\alpha)\left[(\lambda+2\mu)A_{y}\bar{l}_{y}^{\alpha-1}k_{2y}^{\alpha+1}e_{2} + \mu A_{y}\bar{l}_{x}^{\alpha-1}k_{2x}^{\alpha+1}e_{2} + \lambda A_{x}\bar{l}_{x}^{\alpha-1}k_{1x}^{\alpha-1}k_{1y}e_{1} + \mu A_{x}\bar{l}_{y}^{\alpha-1}k_{1y}^{\alpha-1}k_{1x}e_{1}\right]$$

$$(4.3b)$$

where $\bar{l}_j^{\alpha-1} = \frac{1}{2}(l_{A_j}^{\alpha-1} + l_{B_j}^{\alpha-1})$ and for brevity, we denote $e_1 := \mathrm{e}^{\mathrm{i}(k_1 \cdot x - \omega t)}$ and $e_2 := \mathrm{e}^{\mathrm{i}(k_2 \cdot x - \omega t)}$. To separate the compressional and shear waves, we set $k_{1y} = k_{2y} = 0$ allowing us to let both the wavevectors $k_1 = k_{1x}\hat{x}$ and $k_2 = k_{2x}\hat{x}$ to be along the \hat{x} -direction. The component of the displacement field u(x,t) along the \hat{x} -direction is parallel to the wavevector k_1 and hence gives the field of particles vibrating along the direction of propagation of the wave. This allows us to recover the P wave and to denote $k_{1x} = k_p$. Likewise, the component of the displacement field u(x,t) along the \hat{y} -direction is perpendicular to the wavevector k_2 and hence gives the field of particles vibrating perpendicular to the direction of propagation of the wave. This allows us to recover the S wave and to denote $k_{2x} = k_s$. The complex wavenumbers k_p and k_s are found as:

$$-\rho\omega^2 = i^{\alpha+1}\Gamma(2-\alpha)(\lambda+2\mu)\bar{l}_p^{\alpha-1}k_p^{\alpha+1}$$
(4.4a)

and

$$-\rho\omega^2 = i^{\alpha+1}\Gamma(2-\alpha)\mu \,\bar{l}_s^{\alpha-1}k_s^{\alpha+1}.\tag{4.4b}$$

In equation (4.4), \bar{l}_p and \bar{l}_s are defined the effective horizon lengths along the direction of propagation of the P wave and the S wave, respectively (figure 2). These lengths are given as:

$$\bar{l}_{m}^{\alpha-1} = \frac{1}{2} \left(l_{A_{m}}^{\alpha-1} + l_{B_{m}}^{\alpha-1} \right) \tag{4.5a}$$

and

$$l_{N_m} = \begin{cases} l_{N_x} \sec \theta_m & \theta_m \le \theta_l \ \left(= \tan^{-1} \left(\frac{l_{N_y}}{l_{N_x}} \right) \right) \\ l_{N_y} \csc \theta_m & \theta_m > \theta_l \end{cases}$$
(4.5b)

where $N \subset \{A, B\}$ and $m \subset \{p, s\}$ (p denotes compressional waves and s denotes shear waves). Simplifying equation (4.4) gives the dispersion relations for the non-local medium as:

$$k_m^{(s)} = -i \left[\frac{\bar{l}_m^{1-\alpha}}{\Gamma(2-\alpha)} \right]^{1/(\alpha+1)} \left(\frac{\omega}{V_m} \right)^{2/(\alpha+1)} e^{i\pi/(\alpha+1)}, \tag{4.6}$$

where $V_p\left(=\sqrt{(\lambda+2\mu)/\rho}\right)$ and $V_s(=\sqrt{\mu/\rho})$ are the classical compressional and shear wave speeds in an isotropic bulk solid. In order to differentiate the dispersion relations of the space-fractional and the time-space-fractional wave equations (which we will derive in the following) from each other we use the superscripts $\Box^{(s)}$ and $\Box^{(t)}$, respectively.

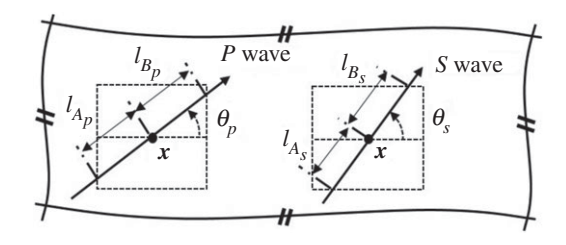


Figure 2. Schematic illustrating the horizon lengths I_{N_n} and I_{N_n} in equation (4.5).

The real and imaginary parts of the complex wave vector $k_m^{(s)}$ correspond to the propagating and attenuating component of the wave. By extracting the imaginary part $\kappa_m^{(s)} = \Im(k_m^{(s)})$ from equation (4.6), we find the attenuation corresponding to the space-fractional formulation to be:

$$\kappa_m^{(s)}(\omega) = \left\lceil \frac{\bar{l}_m^{1-\alpha}}{\Gamma(2-\alpha)} \right\rceil^{1/(\alpha+1)} \left(\frac{\omega}{V_m} \right)^{2/(\alpha+1)} \left| \cos\left(\frac{\pi}{\alpha+1} \right) \right|, \tag{4.7}$$

Noting that $\cos(\pi/(\alpha+1)) < 0 \,\,\forall \,\,\alpha \in (0,1)$, we conclude that space-fractional waves exhibit a power-law frequency-dependent attenuation with index $2/(\alpha+1)$. Since, the index is always positive, it is immediate to conclude that the space-fractional formulation predicts an increase in attenuation with the increasing frequency. The dispersion in terms of the wave speed c_m is:

$$c_m^{(s)}(\omega) = \left[\frac{\Gamma(2-\alpha)}{\overline{l}_m^{1-\alpha}} \right]^{1/(\alpha+1)} \left(\frac{V_m^2}{\omega^{1-\alpha}} \right)^{1/(\alpha+1)} \left| \csc\left(\frac{\pi}{\alpha+1}\right) \right|. \tag{4.8}$$

Noting that $\sin(\pi/(\alpha+1)) > 0 \ \forall \ \alpha \in (0,1)$ the phase velocity decreases as frequency increases, hence indicating anomalous dispersion if compared with traditional dispersion of bulk materials.

Although the present study focuses on the attenuating effects due to the space-fractional terms, we provide for completeness the attenuation and dispersion relations for the time-space-fractional waves. By using the same procedure described above, we obtain the dispersion relations as:

$$k_m^{(t)} = -i \left[\frac{\tau_0^{\beta - 2} \bar{l}_m^{1 - \alpha}}{\Gamma(2 - \alpha)} \right]^{1/(\alpha + 1)} \left(\frac{\omega}{V_m^{\frac{2}{\beta}}} \right)^{\beta/(\alpha + 1)} e^{-i\pi\beta/2(\alpha + 1)}. \tag{4.9}$$

Indicating $\Im(k_m^{(t)}) = \kappa_m^{(t)}$ and noting that $\cos(\pi\beta/2(\alpha+1)) < 0$ for $\alpha \in (0,1)$ and $\beta \in (1,2)$, the attenuation $\kappa_m^{(t)}(\omega)$ for the compressional and shear waves is obtained as:

$$\kappa_m^{(t)}(\omega) = \left[\frac{\tau_0^{\beta - 2} \bar{l}_m^{1 - \alpha}}{\Gamma(2 - \alpha)} \right]^{1/(\alpha + 1)} \left(\frac{\omega}{V_m^{\frac{2}{\beta}}} \right)^{\beta/(\alpha + 1)} \left| \cos\left(\frac{\pi \beta}{2(\alpha + 1)}\right) \right|. \tag{4.10}$$

Clearly, the time-space-fractional wave follows power-law attenuation with attenuation index $\beta/(\alpha+1)$ for ω . Again, a positive value of the power-law index indicates that the time-space-fractional formulation predicts an increase in attenuation with frequency. Noting that $\sin(\pi\beta/2(\alpha+1)) > 0 \ \forall \ \alpha \in (0,1)$ and $\beta \in (1,2)$, the dispersion in the wave speeds is given by:

$$c_m^{(t)}(\omega) = \left[\frac{\Gamma(2-\alpha)}{\tau_0^{\beta-2} \bar{l}_m^{1-\alpha}} \right]^{1/(\alpha+1)} \left(\frac{V_m^2}{\omega^{\beta-1-\alpha}} \right)^{1/(\alpha+1)} \left| \csc\left(\frac{\pi\beta}{2(\alpha+1)} \right) \right|. \tag{4.11}$$

It follows that the phase velocity decreases as frequency increases, hence indicating anomalous dispersion if compared with traditional dispersion of bulk local materials. Note also that, the attenuation–dispersion terms of both the space-fractional and time-space-fractional wave equations form a Hilbert pair confirming that the wave equations are causal [16,17].

(a) Equivalent fractional model of a non-local solid

Consider a material with attenuation described by $\kappa = \kappa_0 |\omega|^{\gamma}$ for the P wave or the S wave, where κ_0 and γ are constants characterizing the medium. The equivalent non-local (fractional) representation is found by comparing the power-law behaviour of the material with equation (4.7). The non-local parameters α and \bar{l}_m are found as:

$$\alpha = \frac{2 - \gamma}{\gamma} \tag{4.12a}$$

and

$$\bar{l}_{m} = \left[\kappa_{0} V_{m}^{\gamma} \middle| \sec\left(\frac{\pi \gamma}{2}\right) \middle| \right]^{1/(\gamma - 1)} \left[\Gamma\left(3 - \frac{2}{\gamma}\right)\right]^{\gamma/2(\gamma - 1)}. \tag{4.12b}$$

Thus, for a given medium the length scale and the order are related. Note that as $\gamma \to 1$, $\alpha \to 1$ and \bar{l}_m is undefined, which means that we recover the local formulation.

A particularly striking outcome of the space-fractional model is that since $\alpha \in (0,1)$ equation (4.12*a*) leads to the restriction that $\gamma \in (1,2)$. Indeed, a majority of the experiments on practical materials has so far established that the attenuation exponent $\gamma \in (1,2)$ [16,36,37]. For example, attenuation of compressional waves by underground sediments and layered rocks are found to correspond to $\gamma \approx 1$ [50,51]. Attenuation exponents of $\gamma \in (1,2)$ were observed in human tissues [52], and fluids such as distilled water and certain oils [53]. In high-frequency regimes, certain materials like plastics (e.g. lexan), low- and high-density polyethylene, and aerogels exhibit attenuation with exponent $\gamma \in (0,1)$ [16,37,54]. This behaviour is captured by the time-space-fractional wave equation which allows the attenuation exponent γ to vary in (0,1) (equation (4.10)). This short discussion on practical materials exhibiting anomalous attenuation highlights that the fractional formulation could be essential to model these complex materials.

Note that both attenuation and dissipation affect the dispersion relation by inducing a power-law dependence in frequency. Hence, in practical experiment it is not immediate to discern what physical mechanism lies behind the occurrence of fractional dispersion. However, based on the mathematical formulation presented above, it is clear that space-fractional operators are indicative of attenuation in conservative media whereas time-fractional operators imply dissipation in non-conservative media [1,4,5,39]. Note also that, in the purely space-fractional case the attenuation (equation (4.7)) is a fractional-order power-law function of the wavenumber. While in the purely time-fractional case (i.e. for $\alpha=2$ and $\beta\in(1,2)$ in equation (4.10)), the attenuation is a fractional-order power-law function of frequency only. Thus, based on available experimental data, one could determine if the solid should be modelled via either space-fractional or time-fractional operators (or a combination of them as in equation (4.10)), by assessing whether it exhibits a wavelength-based or frequency-based power-law attenuating behaviour. A double Fourier transform of a transient response would provide these data. Then, the fractional-order can be obtained by a power-law fit of the distribution.

5. Non-local interfaces: Snell's Law and Fresnel's coefficients

A key question to understand the propagation of elastic waves in complex non-local media concerns the effect of interfaces between media having different constitutive behaviour. Consider, as an example, an interface between a local and a non-local medium or between two different non-local media. The first case can be modelled as an integer–fractional interface, while the second as a fractional–fractional one. The local–non-local interface represents the most general case, and hence it is selected as a benchmark example for the following analyses.

In classical wave analysis, the interaction of plane waves with planar interfaces is fully characterized by Snell's Law (which provides the angle of propagation of the reflected and refracted waves) and Fresnel's coefficients (which allow determining the amplitude of the reflected and refracted wave fronts). Consider the interface between a local (solid #1, α = 1) and a non-local (solid #2, $0 < \alpha < 1$) isotropic bulk elastic solid (figure 3). An incident *P*-type plane

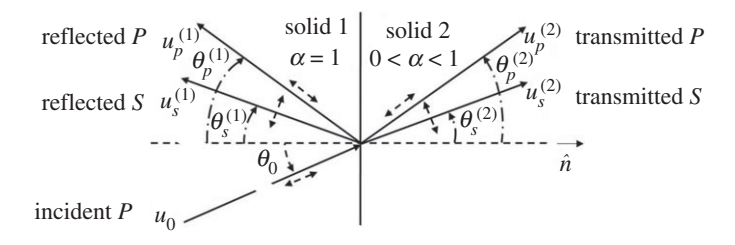


Figure 3. Schematic of the interface between the local ($\alpha = 1$) and the non-local ($0 < \alpha < 1$) elastic bulk medium. Given an incident P wave, the possible wave types and angles of reflection and refraction are identified. The dashed double arrow indicates the polarization of the wave.

wave travels from the local to the non-local medium. By leveraging the previously introduced elastodynamic model, we extend Snell's Law to account for this type of mixed local–non-local interfaces. Enforcing the continuity of displacement and traction at the interface gives:

$$u = u_0 + R_{pp}u_p^{(1)} + R_{ps}u_s^{(1)} = T_{pp}u_p^{(2)} + T_{ps}u_s^{(2)}$$
(5.1a)

and

$$\tilde{t} = \tilde{t}_0 + \tilde{t}_p^{(1)} + \tilde{t}_s^{(1)} = \tilde{t}_p^{(2)} + \tilde{t}_s^{(2)}, \tag{5.1b}$$

where R_{pp} , R_{ps} , T_{pp} and T_{ps} are reflection and transmission coefficients of P and S waves (for an incident P wave). u_0 , $u_p^{(1)}$, $u_s^{(1)}$, $u_p^{(2)}$ and $u_s^{(2)}$ are displacement polarization vectors for the incident, reflected, and transmitted waves, as shown in figure 3. The superscripts $\Box^{(1)}$ and $\Box^{(2)}$ indicate the medium supporting the wave, hence $\Box^{(1)}$ refers to reflected waves and $\Box^{(2)}$ refers to transmitted waves. The corresponding tractions are denoted as \tilde{t}_0 , $\tilde{t}_p^{(1)}$, $\tilde{t}_s^{(1)}$, $\tilde{t}_p^{(2)}$ and $\tilde{t}_s^{(2)}$. The angles of the incident, reflected and refracted waves measured with respect to the normal to the interface are denoted as θ_0 , $\theta_p^{(1)}$, $\theta_s^{(1)}$, $\theta_p^{(2)}$ and $\theta_s^{(2)}$.

The continuity of the displacement field along the interface holds at all time instants and leads to the following relation between the wavenumbers of the P/S waves at the interface:

$$k_0 \sin \theta_0 = k_p \sin \theta_p^{(1)} = k_s \sin \theta_s^{(1)} = k_p^{\alpha} \sin \theta_p^{(2)} = k_s^{\alpha} \sin \theta_s^{(2)},$$
 (5.2)

where k_0 , k_p and k_s are wavenumbers of the incident P wave, and reflected P and S waves, while k_p^{α} and k_s^{α} are wavenumbers of the transmitted P and S wave within the non-local medium. By combining equation (5.2) with equation (4.8), we obtain:

$$\sin \theta_m^{(1)} = \frac{V_m^{(1)}}{V_p^{(1)}} \sin \theta_0 \tag{5.3a}$$

and

$$\sin \theta_m^{(2)} = \bar{l}_m^{(\alpha-1)/(\alpha+1)} \frac{\omega}{V_p^{(1)}} \left[\frac{\sqrt{\Gamma(2-\alpha)}V_m^{(2)}}{\omega} \right]^{2/(\alpha+1)} \frac{\sin \theta_0}{\sin(\frac{\pi}{\alpha+1})}$$
(5.3b)

where $m \in \{p,s\}$ and $V_p^{(1)}$, $V_s^{(1)}$, $V_p^{(2)}$ and $V_s^{(2)}$ are the classical compressional and shear wave speeds in solid #1 and #2. The length scales \bar{l}_p and \bar{l}_s , vary with $\theta_p^{(2)}$ and $\theta_s^{(2)}$ as given in equation (4.5) and thus, equation (5.3) must be solved numerically. By setting $\sin\theta_p^{(2)}=\sin\theta_s^{(2)}=1$, the first and second critical angles (indicated by θ_p^c and θ_s^c , respectively) are obtained as:

$$\sin \theta_m^c = \frac{\sin(\pi/(\alpha+1))}{\bar{l}_m^{(\alpha-1)/(\alpha+1)}} \left[\frac{V_p^{(1)}}{\omega} \left(\frac{\omega}{\sqrt{\Gamma(2-\alpha)} V_m^{(2)}} \right)^{2/(\alpha+1)} \right]. \tag{5.4}$$

For an incident *P* wave, equation (5.1) can be recast in a matrix form as:

$$\begin{bmatrix} \cos \theta_{p}^{(1)} & -\sin \theta_{s}^{(1)} & \cos \theta_{p}^{(2)} & \sin \theta_{s}^{(2)} \\ \sin \theta_{p}^{(1)} & \cos \theta_{s}^{(1)} & -\sin \theta_{p}^{(2)} & \cos \theta_{s}^{(2)} \\ \lambda_{1} + 2\mu_{1} \cos^{2} \theta_{p}^{(1)} & -\mu_{1} \sin 2\theta_{p}^{(1)} & A_{33} & A_{34} \\ \sin 2\theta_{p}^{(1)} & \frac{V_{p}^{(1)}}{V_{s}^{(1)}} \cos 2\theta_{s}^{(1)} & A_{43} & A_{44} \end{bmatrix} \begin{bmatrix} R_{pp} \\ R_{ps} \\ T_{pp} \\ T_{ps} \end{bmatrix} = \begin{bmatrix} \cos \theta_{0} \\ -\sin \theta_{0} \\ -(\lambda_{1} + 2\mu_{1} \cos^{2} \theta_{0}) \\ \sin 2\theta_{0} \end{bmatrix},$$

$$(5.5a)$$

where, λ_1 , μ_1 , λ_2 and μ_2 are the Lamé constants of solid #1 or #2. A_{33} , A_{34} , A_{43} and A_{44} are:

$$A_{33} = \bar{A} \left[(\lambda_2 + 2\mu_2) \bar{l}_x^{\alpha - 1} \cos \theta_p^{(2)} \cot^{\alpha} \theta_p^{(2)} + \lambda_2 \bar{l}_y^{\alpha - 1} \sin \theta_p^{(2)} \right], \tag{5.6a}$$

$$A_{34} = \bar{A} \left[(\lambda_2 + 2\mu_2) \bar{l}_x^{\alpha - 1} \sin \theta_s^{(2)} \cot^{\alpha} \theta_s^{(2)} - \lambda_2 \bar{l}_y^{\alpha - 1} \sin \theta_s^{(2)} \right], \tag{5.6b}$$

$$A_{43} = -\bar{A} \left(\frac{\mu_2}{\mu_1} \right) \left[\bar{l}_x^{\alpha - 1} \sin \theta_p^{(2)} \cot^{\alpha} \theta_p^{(2)} + \bar{l}_y^{\alpha - 1} \cos \theta_p^{(2)} \right]$$
 (5.6c)

and

$$A_{44} = -\bar{A} \left(\frac{\mu_2}{\mu_1} \right) \left[-\bar{l}_x^{\alpha - 1} \cos \theta_s^{(2)} \cot^{\alpha} \theta_s^{(2)} + \bar{l}_y^{\alpha - 1} \sin \theta_s^{(2)} \right], \tag{5.6d}$$

with \bar{A} given as: $\bar{A} = -\Gamma(2-\alpha)k_0^{\alpha-1}\sin(\pi/2\alpha)(\sin\theta_0)^{\alpha}$. As expected, for $\alpha=1$ the classical form of both Snell's Law and the Fresnel coefficients are recovered.

The formulation presented above allows for some preliminary observations on the effect of non-locality on the wave scattering process. Consider a situation where solid #1 is local and solid #2 is non-local, but both have the same elastic constants (e.g. they both are made out of steel having Young's modulus $E = 200 \,\mathrm{GPa}$ and Poisson's ratio $\nu = 0.29$). We investigate the effect of the degree of non-locality on the wave scattering by plotting equation (5.3) for different combinations of order α and length-scale l in figure 4. When $\alpha \to 1$ and $l \to 0$ the refraction angle of the P wave approaches the results of classical Snell's Law, as expected. When both solids are local ($\alpha = 1$), there is neither mode conversion or scattering because the interface vanishes giving rise to a uniform continuous medium. As the degree of non-locality of solid #2 increases (by decreasing α or increasing l [43]), the refracted P/S waves progressively bend towards the normal to the interface indicating a consistent softening of the solid. Further, the transmitted waves are attenuated in the non-local solid. It follows that, with increasing degree of nonlocality, the interface evolves from high transmissibility (local to local) to high reflectivity (local to non-local). We merely note that such behaviour is typical of solids subject to high temperature gradients where non-local effects are prominent and thermo-rheological properties are strongly affected [6].

6. Validation studies

In this section, we proceed to the validation of the fractional-order elastodynamic model by following a twofold approach. First, we numerically solve the fractional-order continuum model to simulate the wave interaction with a local-to-non-local interface. The numerical results are compared with the predictions from the non-local Snell's Law. This step is intended to confirm the validity of the equivalent (fractional) non-local Snell's Law extracted from the underlying elastodynamic model. Certainly, given that Snell's Law itself is derived from the same model used for the numerical simulations, these results are not sufficient to validate the elastodynamic model itself. In order to address this latter aspect of the validation process, we select a practical example of a physical system that can be effectively described by the fractional elastodynamic model and present a semi-analytical approach to obtain the fractional-order that describes the physical medium. The details of this two-step validation strategy are presented here below.

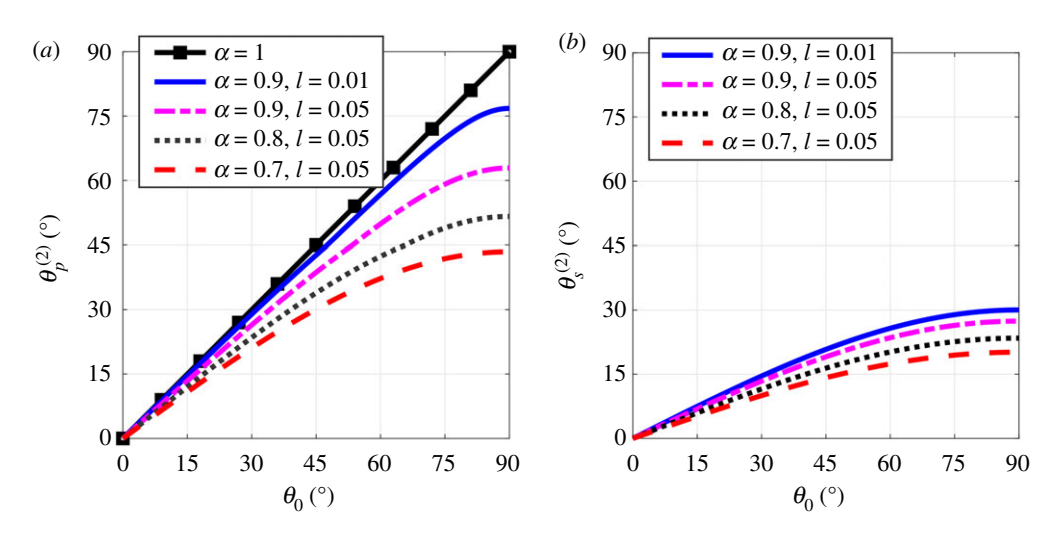


Figure 4. Theoretical predictions of the variation of the refraction angles (a) $\theta_p^{(2)}$ and (b) $\theta_s^{(2)}$ assuming an incident P wave on a local—non-local interface. Elastic constants of steel and excitation frequency f=100 kHz are assumed for the calculations. The non-local interface progressively bends the waves towards the normal to the interface with increasing non-local behaviour. (Online version in colour.)

(a) Validation of the non-local Snell's Law

In order to validate the theoretical formulation of the non-local Snell's Law, we solved equation (3.1) numerically and compared the observed scattering behaviour with the theoretical predictions. The numerical solution of the non-local elastodynamic model was obtained by finite difference (details provided in electronic supplementary material). The simulations were performed assuming an interface between a local and a non-local isotropic medium. The non-local character of a solid is typically connected to its internal microstructure whose length-scale varies across classes of materials [24]. The effect of the length-scale on the material dynamics has been experimentally captured for several classes of materials including aluminium, copper and nickel [55]. The sources of non-locality include, among others, heterogeneity of the microstructure, presence of distributed cracks and metal plasticity [24], and even periodic material or geometric inclusions [1,39]. A specific example belonging to the latter class of systems will be shown in §6b. Here, we choose cadmium as the classical medium and steel as the non-local medium. The specific selection of these materials was mostly driven by the need to produce a sufficient discontinuity in the mechanical impedance of the layers so as to produce appreciable scattering at the interface and to achieve both critical angles.

As numerical benchmark case, we considered the 2D domain $0.5 \times 0.25\,\mathrm{m}^2$ shown in figure 5 including an interface between local cadmium (solid #1; $V_p = 2790\,\mathrm{m\,s^{-1}}$, $V_s = 1490\,\mathrm{m\,s^{-1}}$ and $\alpha = 1$) and non-local steel (solid #2; $V_p = 5990\,\mathrm{m\,s^{-1}}$, $V_s = 3200\,\mathrm{m\,s^{-1}}$, $\alpha = 0.9$ and isotropic horizon $0.025 \times 0.025\,\mathrm{m}^2$). A single quasi-planar P-wave burst with centre frequency $f_c = 100\,\mathrm{kHz}$ and with an angle of incidence θ_0 was selected as excitation. The incident wave was generated by the application of an external force on a straight line of length $0.16\,\mathrm{m}$. The wave burst was obtained by applying a Hanning window to a sine wave with the prescribed centre frequency f_c . This strategy helps focusing most of the energy at the centre frequency, thereby reducing the presence of spurious harmonics due to the initial transience. Further, we imposed fixed boundary conditions on all edges. All the simulations presented here below were conducted in the time domain so that boundary reflections could be easily eliminated by a time-gating process.

The first and second critical angles for the system were obtained from equation (5.4) as 29° and 69.3°, respectively. Based on these values, the system was simulated in four different regimes, that is $\theta_0 < \theta_p^c$, $\theta_0 = \theta_p^c$, $\theta_p^c < \theta_0 < \theta_s^c$ and $\theta_0 = \theta_s^c$. The corresponding values of θ_0 are: 20°, 29°, 45° and

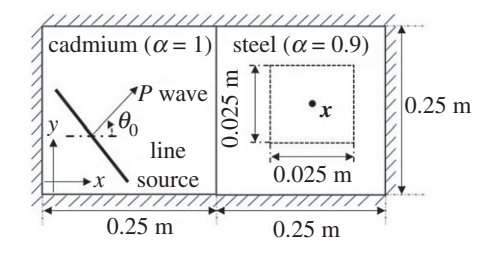


Figure 5. Schematic of the computational domain used to numerically validate the analytical predictions provided by the non-local Snell's Law (not to scale).

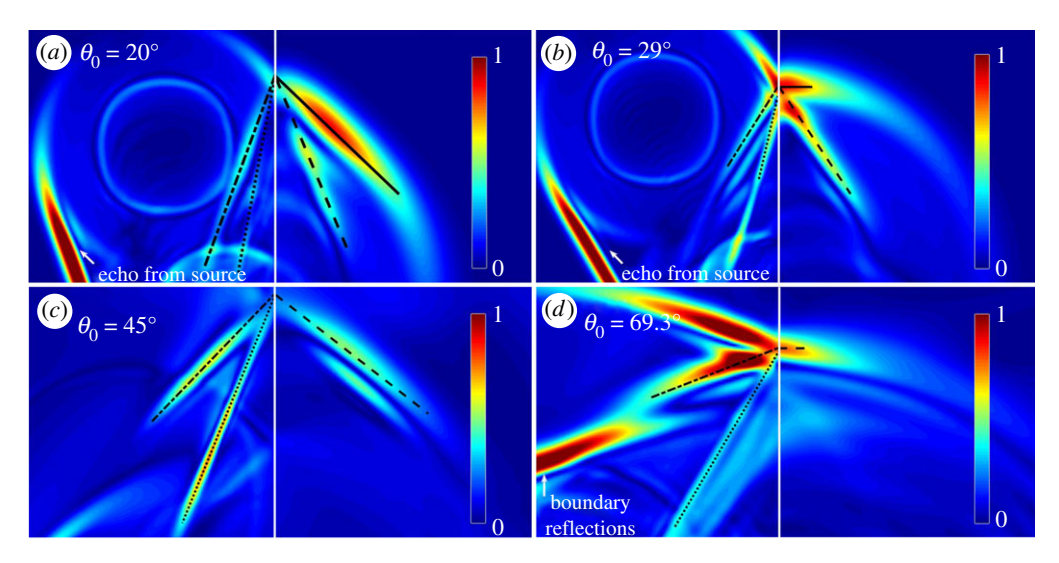


Figure 6. Numerical simulations showing the interaction of a P wave with the interface between the local and non-local medium in figure 5. The solid white line denotes the interface. The black lines show the main wave fronts after the interaction with the interface; solid line: refracted P wave, dashed line: refracted P wave, dotted line: reflected P wave, and dashed-dot line: reflected P wave. (a) $P_0 < P_0^c$ both P and P waves are generated. (b) $P_0 = P_0^c$: the transmitted P wave travels along the interface. (c) $P_0^c < P_0^c$ only the mode-converted P wave is transmitted. (d) $P_0 = P_0^c$: the mode-converted P wave is perpendicular to the interface normal. The low intensity waves that can still be observed in solid #2 are due to the finite nature of the line source which produces spurious non-planar components at its edges. (Online version in colour.)

 69.3° . Figure 6 shows the numerically evaluated elastic wave fields, after interaction with the interface. The P/S waves were identified from the relation between the direction of the wave and particle velocities (electronic supplementary material, figure S1). Curve fitting was used to extract the angles of reflection and transmission. Theoretical and numerical predictions are compared in table 1. As evident from the absolute errors, numerical results show an excellent agreement with the non-local Snell's Law.

(b) Validation of fractional-order continuum model for non-local solids

In the previous section, we pointed out that many materials of practical interest show non-local effects, mostly due to different types of inhomogeneities present at microstructural level. Despite the existence of experimental data corroborating both the existence and the importance of non-local effects in selected media, their connection with specific material parameters (that is of paramount importance for numerical simulations) is still a challenging topic. For this reason, we present an alternative material system that is characterized by non-local effects induced by

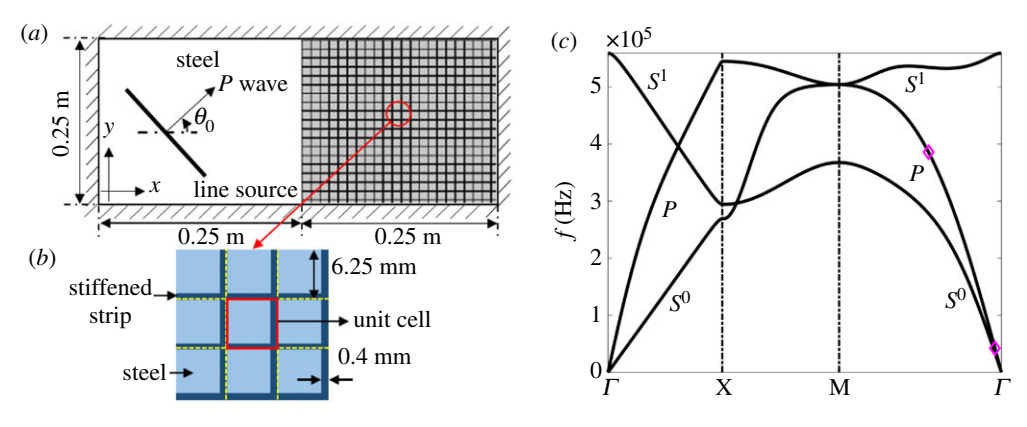


Figure 7. (*a*) Schematic of the computational domain used to validate the analytical predictions of the generalized elastodynamic model. (*b*) The super-cell used to construct the solid #2. The unit-cell is highlighted in red and its dimensions are specified. (*c*) Dispersion curves for the periodic solid in (*b*) plotted along the irreducible part of the first Brillouin zone. *P* denotes the longitudinal mode, and S^0 and S^1 represent the shear modes. The two points marked in ' \diamondsuit ' were used to extract the parameters α and *I* using equations (6.1) and (6.2). (Online version in colour.)

Table 1. Comparison of the theoretical and numerical predictions of reflection and refraction angles for various regimes of incidence θ_0 and the relative error between them in percentage.

	Snell's Law				finite difference				error in percentage			
$ heta_{ extsf{0}}$	$\theta_p^{(1)}$	$ heta_{s}^{ ext{(1)}}$	$\theta_p^{(2)}$	$\theta_s^{(2)}$	$\theta_p^{(1)}$	$ heta_{s}^{(1)}$	$\theta_p^{(2)}$	$\theta_s^{(2)}$	$\overline{\theta_p^{(1)}}$	$\theta_s^{(1)}$	$\theta_p^{(2)}$	$\theta_{s}^{(2)}$
20	20	10.5	44.2	21.5	20	11	45	22	0	4.8	1.8	2.3
29	29	15.0	90	30.9	29	15.6	90	31	0	4	0	0.3
45	45	22.2	—	48.1	45.6	23	—	49	0	4	0	0.3
69.3	69.3	30.0		90	68	31	—	90	1.9	3.3	0	0

the macrostructural configuration. This material system offers an ideal benchmark to validate the fractional-order elastodynamic model as well as its ability to describe practical physical systems. The system under investigation is shown in figure 7 and consists of an interface between an isotropic homogeneous medium and a non-homogeneous medium. The latter is realized by embedding a square grid of a stiffer material into a more compliant background. Although we use a plane strain model in this study, this configuration can be considered representative of a classical thin walled panel with a square grid of stiffeners. This material system is of particular interest because its dynamic response can be simulated using a traditional finite element technique without requiring any assumption on either length scales or microstructural properties.

We consider a 2D domain of size $0.5 \times 0.25 \,\mathrm{m}^2$, as shown in figure 7a. The two subdomains are made out of steel (solid #1; $E_1 = 205 \,\mathrm{GPa}$ (Young's modulus), $v_1 = 0.3$ (Poisson's ratio), and $\rho_1 = 7700 \,\mathrm{kg} \,\mathrm{m}^{-3}$ (density)) and a stiffened medium (solid #2). The stiffened medium consists in a steel background an embedded square grid of a stiffer material: $E_2 = 10 \,250 \,\mathrm{GPa} = 50 E_1$, $v_2 = 0.3$ and $\rho_2 = 7700 \,\mathrm{kg} \,\mathrm{m}^{-3}$. The dimensions of the unit-cell are illustrated in figure 7b. In order to be able to use the fractional-order elastodynamic model to predict the scattering behaviour in such system, we need a procedure to estimate the fractional model parameters, order α and length scale l, corresponding to the non-local solid #2. The specific configuration chosen for solid #2 offers a very viable approach to extract these parameters. Solid #2 can be seen as a periodic medium having a lattice constant $a = 6.25 \,\mathrm{mm}$. The infinite medium constructed from this unit cell is associated with a specific dispersion behaviour which can be calculated numerically by solving the eigenvalue problem based on the Navier's equations describing the medium. This calculation was performed

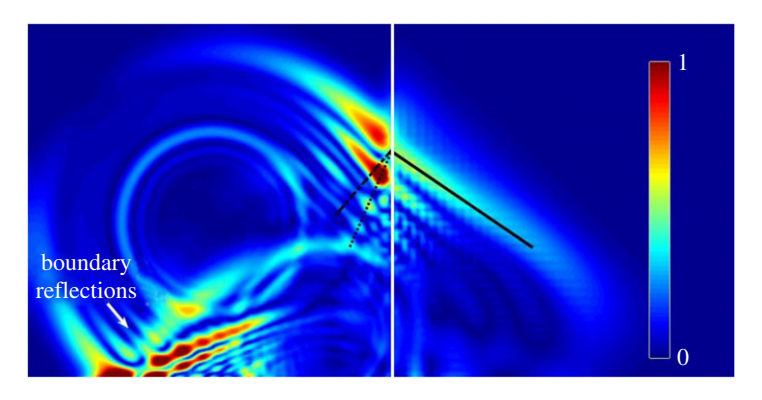


Figure 8. Numerical simulations performed in COMSOL showing the interaction of a *P* wave with an interface between the local and the periodically stiffened medium. The lines used to indicate the different wave fronts are the same as described for figure 6. (Online version in colour.)

using COMSOL Multiphysics and the results are shown in figure 7*c* in terms of the irreducible part of the first Brillouin zone.

Having the numerical dispersion curves available, we can extract the parameters α and l by fitting the power-law behaviour given in equation (4.6) against the numerical data. More specifically, the fractional model parameters are extracted from the dispersion curve corresponding to the Γ – M direction of the longitudinal mode which captures the situation of a wave impinging on the local–non-local interface at an angle of 45°. Selecting two pairs of points (k_1,f_1) and (k_2,f_2) (k_{\square} is the magnitude of the wave-vector, f_{\square} is the frequency, and $\square \in \{1,2\}$) on the longitudinal mode, the fractional parameters can be extracted by fitting the power-law behaviour in equation (4.6). More specifically, we extract the order α by taking the logarithm of both sides of the dispersion relation in equation (4.6). Then we extract the order from the slope of the log k-log f relation as:

$$\alpha = 2 \left[\frac{\log f_2 - \log f_1}{\log k_2 - \log k_1} \right] - 1. \tag{6.1}$$

Substituting the order derived above in equation (4.6) gives the length scale l as:

$$l = [\Gamma(2-\alpha)]^{1/(1-\alpha)} \left(\frac{V_p}{2\pi f_1}\right)^{2/(1-\alpha)} \left[k_1 \csc\left(\frac{\pi}{\alpha+1}\right)\right]^{(1+\alpha)/(1-\alpha)}.$$
 (6.2)

The specific pairs chosen in the computation were $k_{x1} = k_{y1} = 20.11 \,\mathrm{m}^{-1}$ and $f_1 = 42.3 \,\mathrm{kHz}$, and $k_{x2} = k_{y2} = 226.19 \,\mathrm{m}^{-1}$ and $f_2 = 385.7 \,\mathrm{kHz}$ (figure 7c). Using equations (6.1) and (6.2), the fractional parameters were evaluated as $\alpha = 0.82$ and l = 0.72. The compressional wave speed V_p in solid #2 used in equation (6.2) was calculated using the expression: $V_p = \sqrt{[E(1-\nu)]/[\rho(1+\nu)(1-2\nu)]}$. The stiffness of the non-local solid was obtained as $E = 901 \,\mathrm{GPa}$ using a Rank-2 composite model [56]. Since both the density and Poisson's ratio of the stiffener were chosen to be equal to that of steel, they remain the same for the unit-cell and consequently for the non-local solid.

We now validate the accuracy of the fractional model parameters obtained for solid #2 by simulating the scattering of a P-wave at the interface of solid #1 and solid #2 in COMSOL and comparing the obtained scattering angles with the predictions made from the fractional elastodynamic model. In the simulation set-up, a quasi-planar P-wave incident at an angle $\theta_0 = 45^\circ$ and frequency $f = 300 \, \mathrm{kHz}$ was selected as the source of excitation as shown in figure 7a. The spatial and temporal features of the incident wave are the same as has been described in §6a.

Using the non-local Snell's Law in equation (5.3) and the fractional parameters $\alpha = 0.82$ and l = 0.72, the scattering angles for the set-up shown in figure 7a are found as $\theta_p^{(2)} = 58^\circ$, $\theta_p^{(1)} = 45^\circ$ and $\theta_s^{(1)} = 22.2^\circ$. In order to validate this prediction, we perform a full field time-domain simulation of the set-up shown in figure 7a. The results are shown in figure 8. By curve fitting the reflected and

refracted wave fronts, the scattering angles are obtained as $\theta_p^{(2)} = 57^\circ$, $\theta_p^{(1)} = 43^\circ$ and $\theta_s^{(1)} = 21.9^\circ$. It appears that the predictions of the fractional-order elastodynamic model match very closely the direct simulations obtained from an integer-order and physically realizable structural model. This result completes the validation of the fractional-order elastodynamic model and confirms its ability to capture the response of non-local solids. It is worth noting that the procedure of replacing an integer-order inhomogeneous solid with a fractional-order homogeneous solid effectively results in a homogenization approach where space-fractional derivatives are used to capture the effect of inhomogeneities on a global scale.

7. Conclusion

We presented a generalized non-local elastodynamic theory based on fractional-order differintegral operators and extended the concept of Snell's Law to non-local interfaces. This continuum theory can capture a variety of unconventional transport mechanisms that are of great importance to enable the next generation of predictive tools for many real world applications. Of particular relevance is the ability to account for non-locality (associated with multiscale effects), hybrid and anomalous transport, frequency- and wavelength-dependent dissipation and attenuation effects, and memory (when time-fractional derivative are included). Remarkably, this spacefractional continuum formulation can be interpreted as a fractional homogenization approach that is capable of maintaining the many complex dependencies of the underlying material system due to either spatial or temporal multiscale behaviour. This elastodynamic theory provides the basis for the formulation of a non-local Snell's Law, including closed-form expressions for critical angles and Fresnel's coefficients, hence providing an indispensable tool to design material interfaces between local and non-local media. The fractional-order model was validated against a practical non-local material characterized by macrostructural inhomogeneities. Numerical simulations performed via traditional finite elements matched closely the predictions obtained by the fractional model hence providing a complete validation of both the elastodynamic model and the non-local Snell's Law. It is expected that these results could provide an important foundation to significantly impact predictive capabilities in a variety of applications ranging from continuum mechanics, to elastography, to seismology, to biomedics.

Data accessibility. The additional data in the form of equations supporting this article have been uploaded as part of the electronic supplementary material.

Authors' contributions. S.P. lead the development of the mathematical formulation and of the numerical simulations. F.S. conceived the study and supported the development of the mathematical formulation. Both authors contributed equally to writing the manuscript.

Competing interests. We declare we have no competing interests.

Funding. The authors gratefully acknowledge the financial support of the National Science Foundation (NSF) under grant nos. MOMS 1761423 and DCSD 1825837, and of the Defense Advanced Research Project Agency (DARPA) under grant no. D19AP00052.

Disclaimer. The material presented in this paper is approved for public release; distribution is unlimited. The content of the information does not necessarily reflect the position or the policy of the Government.

References

- 1. Buonocore S, Sen M, Semperlotti F. 2019 Occurrence of anomalous diffusion and non-local response in highly-scattering acoustic periodic media. *New J. Phys.* **21**, e33011.
- Havlin S, Ben-Avraham D. 1987 Diffusion in disordered media. Adv. Phys. 36, 695–798. (doi:10.1080/00018738700101072)
- 3. Mainardi F. 1996 Fractional relaxation-oscillation and fractional diffusion-wave phenomena. *Chaos, Solitons & Fractals* **7**, 1461–1477. (doi:10.1016/0960-0779(95)00125-5)
- 4. Mainardi F. 2010 Fractional calculus and waves in linear viscoelasticity: an introduction to mathematical models. Singapore: World Scientific.
- 5. Chen W, Holm S. 2003 Modified Szabo's wave equation models for lossy media obeying frequency power law. *J. Acoust. Soc. Am.* 114, 2570–2574. (doi:10.1121/1.1621392)

- 6. Povstenko Y. 2015 Fractional thermoelasticity, vol. 219. Berlin, Germany: Springer.
- 7. Benson DA, Wheatcraft SW, Meerschaert MM. 2000 Application of a fractional advection-dispersion equation. *Water Resour. Res.* **36**, 1403–1412. (doi:10.1029/2000WR900031)
- 8. Benson DA, Schumer R, Meerschaert MM, Wheatcraft SW. 2001 Fractional dispersion, Lévy motion, and the MADE tracer tests. *Transp. Porous Media* **42**, 211–240. (doi:10.1023/A:1006733002131)
- 9. Gurevich B, Lopatnikov S. 1995 Velocity and attenuation of elastic waves in finely layered porous rocks. *Geophys. J. Int.* **121**, 933–947. (doi:10.1111/j.1365-246X.1995.tb06449.x)
- 10. Garg S, Nayfeh A. 1986 Compressional wave propagation in liquid and/or gas saturated elastic porous media. *J. Appl. Phys.* **60**, 3045–3055. (doi:10.1063/1.337760)
- 11. Biot MA. 1956 Theory of propagation of elastic waves in a fluid-saturated porous solid. II. Higher frequency range. *J. Acoust. Soc. Am.* **28**, 179–191. (doi:10.1121/1.1908241)
- 12. Stulov A, Erofeev VI. 2016 Frequency-dependent attenuation and phase velocity dispersion of an acoustic wave propagating in the media with damages. In *Generalized continua as models for classical and advanced materials* (eds H Altenbach, S Forest), pp. 413–423. Berlin, Germany: Springer.
- 13. Berkowitz B, Scher H. 1995 On characterization of anomalous dispersion in porous and fractured media. *Water Resour. Res.* 31, 1461–1466. (doi:10.1029/95WR00483)
- 14. Wang Y, Guo J. 2004 Modified Kolsky model for seismic attenuation and dispersion. *J. Geophys. Eng.* 1, 187. (doi:10.1088/1742-2132/1/3/003)
- 15. Wear KA. 2001 A stratified model to predict dispersion in trabecular bone. *IEEE Trans. Ultrason. Ferroelectr. Freq. Control* **48**, 1079–1083. (doi:10.1109/58.935726)
- 16. Szabo TL. 1994 Time domain wave equations for lossy media obeying a frequency power law. *J. Acoust. Soc. Am.* **96**, 491–500. (doi:10.1121/1.410434)
- 17. Fellah ZEA, Berger S, Lauriks W, Depollier C. 2004 Verification of Kramers–Kronig relationship in porous materials having a rigid frame. *J. Sound Vib.* **270**, 865–885. (doi:10.1016/S0022-460X(03)00636-9)
- 18. Mavko GM. 1980 Velocity and attenuation in partially molten rocks. *J. Geophys. Res.: Solid Earth* **85**, 5173–5189. (doi:10.1029/JB085iB10p05173)
- 19. Ben-Avraham D, Havlin S. 2000 *Diffusion and reactions in fractals and disordered systems*. Cambridge, UK: Cambridge university press.
- Eringen AC. 1972 Linear theory of nonlocal elasticity and dispersion of plane waves. *Int. J. Eng. Sci.* 10, 425–435. (doi:10.1016/0020-7225(72)90050-X)
- 21. Eringen AC, Edelen DGB. 1972 On nonlocal elasticity. *Int. J. Eng. Sci.* **10**, 233–248. (doi:10.1016/0020-7225(72)90039-0)
- 22. Aifantis EC. 2003 Update on a class of gradient theories. *Mech. Mater.* **35**, 259–280. (doi:10.1016/S0167-6636(02)00278-8)
- 23. Peerlings RHJ, Geers MGD, De Borst R, Brekelmans W. 2001 A critical comparison of nonlocal and gradient-enhanced softening continua. *Int. J. Solids Struct.* **38**, 7723–7746. (doi:10.1016/S0020-7683(01)00087-7)
- 24. Bažant ZP, Jirásek M. 2002 Nonlocal integral formulations of plasticity and damage: survey of progress. *J. Eng. Mech.* **128**, 1119–1149. (doi:10.1061/(ASCE)0733-9399(2002)128:11(1119))
- 25. Polizzotto C. 2001 Nonlocal elasticity and related variational principles. *Int. J. Solids Struct.* **38**, 7359–7380. (doi:10.1016/S0020-7683(01)00039-7)
- 26. Lazopoulos KA. 2006 Non-local continuum mechanics and fractional calculus. *Mech. Res. Commun.* **33**, 753–757. (doi:10.1016/j.mechrescom.2006.05.001)
- 27. Sumelka W. 2014 Thermoelasticity in the framework of the fractional continuum mechanics. *J. Therm. Stresses* 37, 678–706. (doi:10.1080/01495739.2014.885332)
- 28. Sumelka W. 2016 Fractional calculus for continuum mechanics–anisotropic non-locality. *Bull. Pol. Acad. Sci. Tech. Sci.* **64**, 361–372. (doi:10.1515/bpasts-2016-0041)
- 29. Carpinteri A, Cornetti P, Sapora A. 2011 A fractional calculus approach to nonlocal elasticity. *Eur. Phys. J. Spec. Top.* **193**, 193. (doi:10.1140/epjst/e2011-01391-5)
- 30. Patnaik S, Sidhardh S, Semperlotti F. 2020 Fractional-order models for the static and dynamic analysis of nonlocal plates. (http://arxiv.org/abs/2002.10244)
- 31. Patnaik S, Sidhardh S, Semperlotti F. 2020 Geometrically nonlinear analysis of nonlocal plates using fractional calculus. *Int. J. Mech. Sci.* 105710. (doi:10.1016/j.ijmecsci.2020.105710)
- 32. Hollkamp JP, Semperlotti F. 2020 Application of fractional order operators to the simulation of ducts with acoustic black hole terminations. *J. Sound Vib.* **465**, 115035. (doi:10.1016/j.jsv.2019.115035)

- 33. Di Paola M, Zingales M. 2008 Long-range cohesive interactions of non-local continuum faced by fractional calculus. *Int. J. Solids Struct.* **45**, 5642–5659. (doi:10.1016/j.ijsolstr.2008.06.004)
- 34. Tarasov VE. 2013 Review of some promising fractional physical models. *Int. J. Mod. Phys. B* **27**, 1330005. (doi:10.1142/S0217979213300053)
- 35. Chen W, Holm S. 2004 Fractional Laplacian time-space models for linear and nonlinear lossy media exhibiting arbitrary frequency power-law dependency. *J. Acoust. Soc. Am.* **115**, 1424–1430. (doi:10.1121/1.1646399)
- 36. Treeby BE, Cox BT. 2014 Modeling power law absorption and dispersion in viscoelastic solids using a split-field and the fractional Laplacian. *J. Acoust. Soc. Am.* **136**, 1499–1510. (doi:10.1121/1.4894790)
- 37. Holm S, Sinkus R. 2010 A unifying fractional wave equation for compressional and shear waves. *J. Acoust. Soc. Am.* **127**, 542–548. (doi:10.1121/1.3268508)
- 38. Cottone G, Di Paola M, Zingales M. 2009 Elastic waves propagation in 1D fractional non-local continuum. *Physica E* **42**, 95–103. (doi:10.1016/j.physe.2009.09.006)
- 39. Hollkamp JP, Sen M, Semperlotti F. 2019 Analysis of dispersion and propagation properties in a periodic rod using a space-fractional wave equation. *J. Sound Vib.* **441**, 204–220. (doi:10.1016/j.jsv.2018.10.051)
- 40. Bažant ZP, Chang TP. 1984 Instability of nonlocal continuum and strain averaging. *J. Eng. Mech.* **110**, 1441–1450. (doi:10.1061/(ASCE)0733-9399(1984)110:10(1441))
- 41. Romano G, Barretta R, Diaco M, de Sciarra FM. 2017 Constitutive boundary conditions and paradoxes in nonlocal elastic nanobeams. *Int. J. Mech. Sci.* 121, 151–156. (doi:10.1016/j.ijmecsci.2016.10.036)
- 42. Romano G, Luciano R, Barretta R, Diaco M. 2018 Nonlocal integral elasticity in nanostructures, mixtures, boundary effects and limit behaviours. *Continuum Mech. Thermodyn.* **30**, 641–655. (doi:10.1007/s00161-018-0631-0)
- 43. Patnaik S, Sidhardh S, Semperlotti F. 2020 A Ritz-based finite element method for a fractional-order boundary value problem of nonlocal elasticity. (http://arxiv.org/abs/2001.06885)
- 44. Sidhardh S, Patnaik S, Ŝemperlotti F. 2020 Thermoelastic response of fractional-order nonlocal and geometrically nonlinear beams. (http://arxiv.org/abs/2003.10215)
- 45. Yang Y, Misra A. 2012 Micromechanics based second gradient continuum theory for shear band modeling in cohesive granular materials following damage elasticity. *Int. J. Solids Struct.* **49**, 2500–2514. (doi:10.1016/j.ijsolstr.2012.05.024)
- 46. Madeo A, Barbagallo G, Collet M, D'agostino MV, Miniaci M, Neff P. 2018 Relaxed micromorphic modeling of the interface between a homogeneous solid and a band-gap metamaterial: new perspectives towards metastructural design. *Math. Mech. Solids* 23, 1485–1506. (doi:10.1177/1081286517728423)
- 47. Giorgio I, De Angelo M, Turco E, Misra A. 2019 A Biot–Cosserat two-dimensional elastic nonlinear model for a micromorphic medium. *Continuum Mech. Thermodyn.* 1–13. (doi:10.1007/s00161-019-00848-1)
- 48. Tarasov VE. 2008 Fractional vector calculus and fractional Maxwell's equations. *Ann. Phys.* **323**, 2756–2778. (doi:10.1016/j.aop.2008.04.005)
- 49. Podlubny I. 1998 Fractional differential equations: an introduction to fractional derivatives, fractional differential equations, to methods of their solution and some of their applications. Mathematics in Science and Engineering, vol. 198. Amsterdam, The Netherlands: Elsevier.
- 50. Wuenschel PC. 1965 Dispersive body waves–an experimental study. *Geophysics* **30**, 539–551. (doi:10.1190/1.1439620)
- 51. Collins MD. 1988 The time-domain solution of the wide-angle parabolic equation including the effects of sediment dispersion. *J. Acoust. Soc. Am.* **84**, 2114–2125. (doi:10.1121/1.397057)
- 52. Szabo TL. 2004 Diagnostic ultrasound imaging: inside out. New York, NY: Academic Press.
- 53. Dunn F, Breyer JE. 1962 Generation and detection of ultra-high-frequency sound in liquids. *J. Acoust. Soc. Am.* **34**, 775–778. (doi:10.1121/1.1918194)
- 54. Szabo TL, Wu J. 2000 A model for longitudinal and shear wave propagation in viscoelastic media. *J. Acoust. Soc. Am.* **107**, 2437–2446. (doi:10.1121/1.428630)
- 55. Stölken JS, Evans A. 1998 A microbend test method for measuring the plasticity length scale. *Acta Mater.* **46**, 5109–5115. (doi:10.1016/S1359-6454(98)00153-0)
- 56. Hassani B, Hinton E. 1998 A review of homogenization and topology optimization I-homogenization theory for media with periodic structure. *Comput. Struct.* **69**, 707–717. (doi:10.1016/S0045-7949(98)00131-X)